

SIMULTANEOUS CONTACTING OF BORON AND PHOSPHORUS DOPED SURFACES WITH A SINGLE SCREEN PRINTING PASTE

Jonas D. Huyeng¹, Alma Spribille¹, Mariana García Prince¹, Li C. Rendler¹, Christian Ebert², Ulrich Eitner¹ and Florian Clement¹

¹Fraunhofer Institute for Solar Energy Systems (ISE), Heidenhofstr. 2, 79110 Freiburg, Germany;

²SCHMID Group, Robert-Bosch-Str. 32-36, 72250 Freudenstadt, Germany

ABSTRACT: The contact formation by screen printed metal pastes is widely employed in standard solar cell production. To expand the use of screen printed electrodes to *n*-type solar cells, both boron and phosphorus doped surfaces need to be contacted. To do so with a single material has some advantages especially for IBC solar cells. In this study we test four different screen printing pastes on different boron and phosphorus dopings and in combination with different silicon nitride thicknesses. Phosphorus doping could be contacted over a wide range of sheet resistances, nitride thicknesses and fast firing conditions, leaving much freedom to target the boron contacts. Boron dopings are successfully contacted with all materials, if no capping silicon nitride layer was present. With silicon nitride capping an AgAl and an Ag paste are found to be suitable choices. The lowest contact resistivities with 100 nm SiN_x capping determined in this study are $\rho_c = 0.5 \text{ m}\Omega \text{ cm}^2$ on phosphorus (Ag) and $\rho_c = 1.8 \text{ m}\Omega \text{ cm}^2$ on boron (Ag) doping with one single paste. These results enable highly efficient homojunction IBC cells at low cost.

Keywords: Contact, Doping, Metallization, Screen Printing, Silicon Solar Cell

1 INTRODUCTION AND MOTIVATION

Screen printing is the most commonly used technique for electrode formation on silicon solar cells [1]. For *p*-type solar cells, firing through (FT) Ag paste is used to contact *n*-type emitter doping, while Al paste is used to alloy *p*-type BSF contacts. As soldering on Al is hampered by its native oxide [2], Ag pads are commonly printed on the rear side in an additional step. For *n*-type solar cells, *p*-type emitters are most commonly formed by boron doping, while *n*-type BSF contacts are formed by phosphorus doping. It is desirable to find suitable screen printing pastes to contact B and P simultaneously, to minimize the number of process steps and necessary material supplies. This is especially true for interdigitated back-contact (IBC) cells, where all electrodes can be placed on the rear side in one single printing step [3].

In this study, we compare four different screen printing pastes from different suppliers. We investigate the influence of doping profile and of silicon nitride thickness on the electrode and contact formation. We also examine the mechanical adhesion. For doping we use atmospheric pressure chemical vapor deposition (APCVD) of doped silicate glasses (BSG, PSG), which can be combined with inkjet hotmelt printing to form local dopings as necessary for IBC cells [4].

2 EXPERIMENTAL

Screen printing of electrodes for simultaneous contacting of boron and phosphorus dopings is very attractive for lean fabrication processes for various *n*-type Si solar cell concepts, notably IBC solar cells. Consequently, many paste manufacturers have tried different material compositions to achieve this goal. In this study, four different pastes from industrial manufacturers are compared (s. Tab. I).

One material is optimized for industrial fire through front side emitter metallization in *p*-type PERC cells, but could potentially also contact boron dopings according to the manufacturer. It will be referred to as “Ag (PERC)” in the following. In contrast, one Ag paste has been specifically designed to achieve the simultaneous contacting of boron and phosphorus dopings, while maintaining fire through (“FT”) properties. This paste

will be referred to as “Ag (FT)”. Another Ag paste was manufactured to only cause very low etching of silicon nitride, so it is only suited for thin nitride layers or additional local contact opening (LCO) processes, which allow independent contact and electrode design. As this material is not directly compatible to standard fast firing oven (FFO) processes we refer to it as a “non-firing through” paste, in short “Ag (NFT)”. The fourth material in this study is a FT AgAl paste, as are currently mostly used for bifacial *n*-type cells with boron emitters (“AgAl (FT)”).

2.1 Sample Fabrication

To vary the dopant profile, we compare different drive-in times $t_{\text{Drive-in}}$ for both, boron and phosphorus APCVD dopant sources. We maintain the same APCVD deposition of the BSG and PSG layers for all diffusions. All wet chemical steps, depositions and diffusion processes are carried out at SCHMID facilities in Freudenstadt.

We deposit the silicate glasses on one side of cleaned 6-inch Cz-Si wafers, which was chemically polished after alkaline texturing. On top of BSG or PSG layers, we deposit silicon dioxide layers (SiO_x) as an additional capping before diffusion, in the same APCVD process. After diffusion, some wafers are capped with silicon nitride (SiN_x) for protection and additional hydrogen passivation by a plasma-enhanced chemical vapor deposition (PECVD) process. The thicknesses of the deposited layers are about 40 nm for BSG and PSG layers, 20 nm for the SiO_x capping and up to 100 nm for the SiN_x.

IBC solar cell precursors can be produced with the same APCVD and PECVD tools. After the BSG/SiO_x

Table I: Compared pastes including composition according to the manufacturer and determined finger conductivity after FFO.

	Use	Ag	Al	$\rho_F (\Omega \cdot \text{m})$
Ag (PERC)	FT	70-90 %	0 %	3.7×10^{-8}
Ag (FT)	FT	80-90 %	0 %	4.1×10^{-8}
Ag (NFT)	NFT	80-90 %	0 %	3.5×10^{-8}
AgAl (FT)	FT	80-90 %	1-3 %	4.4×10^{-8}

deposition, wafers can be masked by an inkjet hotmelt in order to selectively etch BSG/SiO_x and to spatially define the emitter and the BSF. Afterwards, the PSG/SiO_x stack can be deposited on top to perform a co-diffusion of both dopants.

2.2 Test Structures

Screen printing of the four pastes is performed on the homogeneously doped wafers in test patterns suitable for determination of finger and contact resistivity (ρ_F , ρ_C). All screen printing is done on automated industrial printers by EKRA at Fraunhofer ISE's PV-TEC. After printing, wafers are dried in an inline conveyor belt dryer. Notably, we use an equidistant finger structure, without interconnecting busbars for the contact resistivity structures. This is suitable for our study, as we target IBC solar cells without busbar features [5].

Contact formation is done in a Fast-Firing Oven (FFO) by Rehm at different peak temperatures, as detailed in the results. All processes are performed at the same speed of 6 m/min.

As a first test to ensure that the novel screen printing pastes can be integrated into a photovoltaic module, we manually solder wire interconnectors with a copper core diameter of 300 μm and a solder coating (10-15 μm) of Sn62Pb36Ag2). We preheat the samples to 120 °C on a hotplate and solder at 270 °C, using a no-clean flux. Aiming at the IBC structure, we use an electrode design which features fingers with a pitch similar to later solar cell devices, and wider contact pads of (200 × 1000) μm^2 .

2.3 Characterization

Initially, wafers with homogeneous doping and without SiN_x capping layers are mapped by a four point probe tool from PVTools to test the uniformity of the doping. Additionally, an ECV profile is measured to estimate the dopant depth profile in the wafer (s. Fig. 1).

After screen printing and firing, the print is investigated by optical microscopy. Afterwards, the test structures are cut from the wafer and analyzed according to the TLM method [6] on a PVTools setup. Line conductivity is determined by a manual four point probe setup. Finger geometry is measured by laser scanning microscopy.

To mechanically characterize the module interconnection, after copper wires are soldered onto small pads, 90° peel tests are performed to measure the mechanical adhesion, according to DIN EN 50461 [7]. We apply a peak detection algorithm on the resulting force-path diagrams and compare the number of identified peaks to the number of printed pads to determine the relative amount of detected peaks, as an indicator for successfully soldered pads [8]. Also, the mean value of the detected force maxima is calculated.

Microstructural analysis of the contact formation is done by scanning electron microscopy (SEM) after mechanical sawing of the samples across the contact fingers and subsequent ion polishing of the surface directly before the measurement.

3 RESULTS

Two runs of wafers were processed. Initially the print and contact properties on samples featuring different

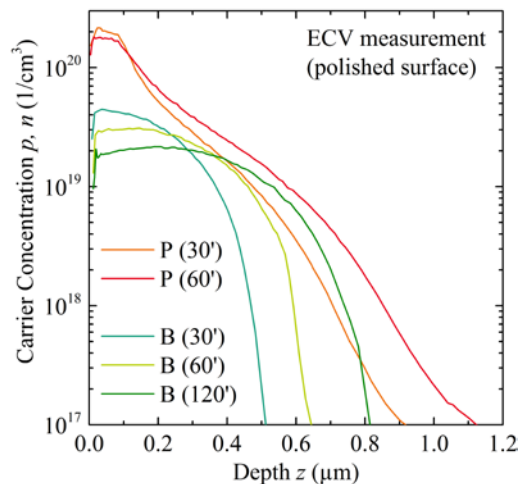


Figure 1: ECV dopant profiles measured on polished samples after APCVD dopant source removal.

dopant profiles with and dielectric layers were tested. In a second run, the drive-in time during diffusion was kept constant and the silicon nitride thickness was varied.

3.1 Finger Geometry after Screen Printing

Results regarding finger width w_F and height h_F of the first print runs on chemically polished wafer surfaces with either BSG/SiN_x or PSG/SiN_x stacks are depicted in Table II. Achieving high aspect ratios on the (polished) wafer surface, especially for the Ag (PERC) and Ag (NFT) turned out to be challenging. Given the previously gathered experience with the Ag (PERC) paste in our laboratory, we question the generality of the found results with regard to this material. Unfortunately, it was not possible to repeat this part of the experiment and we therefore give the (preliminary) determined results for completeness.

In later runs, these results could be improved. Accordingly, all pastes have been deemed feasible for screen printing with appropriate parameters. For IBC solar cells, the finger width does not necessarily need to be reduced below 50 μm , considering that it does not cause any shading losses. On the other hand, wider fingers induce more recombination losses for FT pastes due to wider metal-semiconductor interfaces.

Table II: Finger geometry after initial tests.

	w_F (μm)	h_F (μm)
Ag (PERC)*	42.9 ± 2.8	10.7 ± 2.8
Ag (FT)	49.6 ± 3.0	25.2 ± 3.0
Ag (NFT)*	48.7 ± 1.0	10.6 ± 1.0
AgAl (FT)	50.6 ± 1.0	15.6 ± 1.0

* Visual inspection showed (partly) impaired printing quality.

3.2 Finger and Contact Resistivity

One significant parameter of the electrode grid's series resistance is the finger resistance ρ_F . The determined values by line resistance measurements are given in Tab. I. They have been found to be nearly irrespective of FFO peak temperature.

Another parameter of the series resistance is the metal-semiconductor contact resistivity ρ_C . We determined ρ_C of the screen printed electrodes as a function of the dopant profiles (Fig. 1, Tab. III), as well as the silicon nitride capping thickness ($d_{\text{SiN}_x} = 0, 40, 60, 80, 100$ nm; discussed in 3.3).

The varied dopant profiles (measured by ECV) are given in Fig. 1. A prominent decrease in surface concentration and increase in dopant depth for the boron doping with increasing diffusion time can be found, indicating a limited diffusion source. The phosphorus profiles only show the latter effect (*cf.* Tab. III).

Results for the determined contact resistivity are shown in Fig. 2, for the two dopants (B, P), the varied drive-in time $t_{\text{Drive-in}}$ and three different FFO set temperatures T_{Set} . The box plots indicate the mean (open square), median (center bar), standard deviation (box) and the range 10% - 90% of measured data (whiskers), here and in all following box plots.

We show the data for Ag (FT), Ag (NFT) and AgAl (FT) on bare silicon, which reach satisfying values $\rho_C < 10$ m Ω cm 2 for both dopants and suitable parameter choices (Fig. 2). However, statistic in each group is small (1-5 samples), due to the large number of samples and some breakage during processing. For Ag (FT) we also show the data for wafers with the APCVD dopant sources

Table III: ECV dopant profile characteristics. Given are the drive-in time at maximum temperature, the measured surface concentration and the depth value at a concentration close to the base doping.

	$t_{\text{Drive-in}}$	n_{Surface} (cm $^{-3}$)	z (1×10^{17} cm $^{-3}$) (μm)
P	30'	2.2×10^{20}	0.90
	60'	1.8×10^{20}	1.12
B	30'	4.5×10^{19}	0.50
	60'	3.1×10^{19}	0.64
	120'	2.2×10^{19}	0.80

and an additional 100 nm SiN $_x$ capping layer, tested in the first run (Fig. 2, top right). The data for Ag (PERC) is not displayed, as the results are unexpectedly high even on phosphorus dopings, which indicates that the printing quality negatively affected the results (s. above).

Remarkably, both displayed Ag pastes could reach low values of $\rho_C < 3$ m Ω cm 2 on boron doping (Fig. 2, left). While Ag (FT) also shows very low values of $\rho_C < 1$ m Ω cm 2 on phosphorus doping regardless of FFO set temperature, Ag (NFT) could reach similar values for higher $T_{\text{Set}} \geq 870$ °C. Also, the AgAl (FT) paste (Fig. 2, bottom right) could expectedly reach low values of

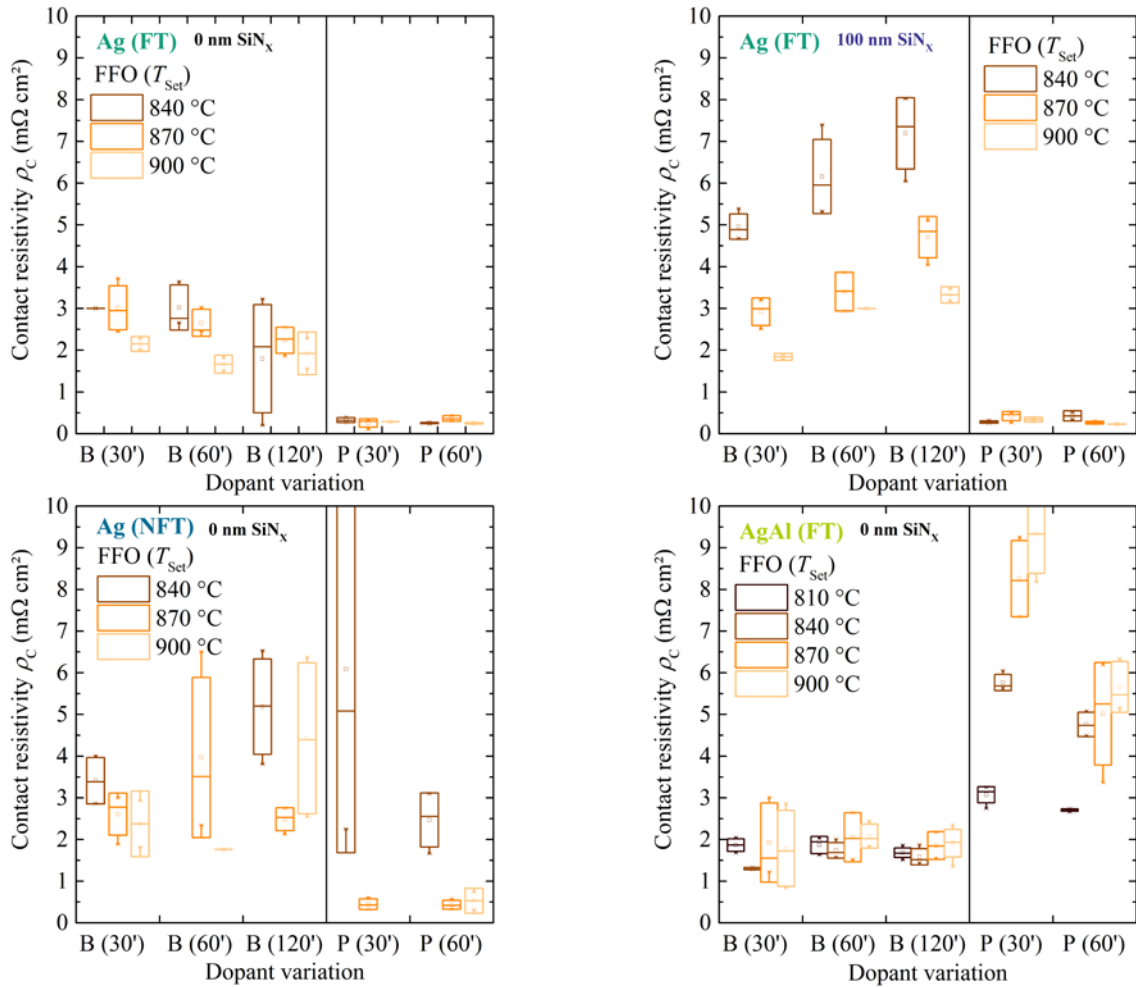


Figure 2: Influence of dopant profile on the contact resistivity for Ag (FT) paste (top, left: without SiN $_x$ layer; top, right: with 100 nm SiN $_x$ layer), Ag (NFT) paste (bottom left: without SiN $_x$ layer) and AgAl (FT) paste (bottom, right: without SiN $_x$ layer).

$\rho_C < 3 \text{ m}\Omega \text{ cm}^2$ on boron doping not correlated with T_{Set} , but only $T_{\text{Set}} \leq 840 \text{ }^\circ\text{C}$ seems suitable for phosphorus doping.

Comparing the results for Ag (FT) on capped and uncapped samples (Fig. 2, top row), it is evident that the addition of the dielectric layers changes contact formation on boron doping, which is much stronger correlated to the thermal budget during the firing process. While at high T_{Set} , similar values can be reached for ρ_C , at lower temperatures the etching of the dielectrics does not seem to be fully successful, resulting in a higher ρ_C . Notably, the capping layers do not influence the contact formation on phosphorus doping.

The trends for Ag (NFT) and AgAl (FT) are the same, but as they exceed $\rho_C > 20 \text{ m}\Omega \text{ cm}^2$ for all tested firing conditions, we chose not to display them here. We assume that the FT properties are also influenced by the polished surface of our samples, as most pastes were probably designed to be used for front side metallization, *i.e.* alkaline textured surfaces.

3.3 Silicon Nitride Thickness Variation

In Fig. 3, we show the trends for the Ag (FT) and Ag (NFT) paste as a function of SiN_x thickness and FFO set temperature. To limit the number of samples, in this run the diffusion time was set at 60 minutes for both boron and phosphorus, targeting a co-diffusion of later cell devices. Again, the Ag (FT) paste showed low contact resistivity $\rho_C < 1 \text{ m}\Omega \text{ cm}^2$ at all conditions, confirming the findings of the first run. A clear dependence on the nitride thickness can be deduced for the Ag (NFT) paste. While an increase of T_{Set} could partly reduce the determined ρ_C , the trend remains even at the highest temperature (920 $^\circ\text{C}$ here, exceeding 900 $^\circ\text{C}$ in the former experiment).

While we refer to Ag (NFT) as a “non-firing through” material, conducted SEM studies of the contacts discussed in the next section reveal small areas where no nitride capping could be identified. One could therefore also refer to it as a “low” or “soft” firing through paste, as the contacting mechanism seems to be the same for this paste. Nevertheless, it is obviously better suited for a setup where contact openings are separately introduced, which leaves room to improve the series resistance of the electrode by printing wider fingers, without dramatically increasing the metal-semiconductor interface.

As in device fabrication the firing process has to be done for both dopings at once, we compiled the best combinations for a given paste in Tab. IV.

Table IV: Best contact resistivities for co-firing without SiN_x capping layer.

	Ag (FT)		Ag (NFT)		AgAl (FT)
FFO T_{Set} ($^\circ\text{C}$)	900	900	900	900	810
$\rho_{C,B}$ ($\text{m}\Omega \text{ cm}^2$)	1.8*	1.7	1.8	1.9	1.9
$\rho_{C,P}$ ($\text{m}\Omega \text{ cm}^2$)	0.5*	0.3	0.5	2.7	

*with 100 nm SiN_x capping

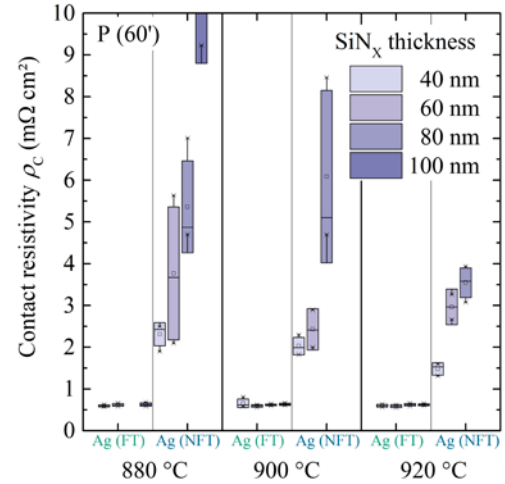


Figure 3: Influence of silicon nitride capping thickness for Ag (FT) and Ag (NFT) on phosphorus doping.

3.4 Microstructural Analysis

To better understand the difference in the contacts, we investigated cross sections of printed and fired fingers by SEM. Three exemplary images are shown for Ag (FT), Ag (NFT) and AgAl (FT) in Fig. 4. Some differences can be seen in the structure of the electrodes (top row) due to the different compositions of the pastes.

Further differences can be seen at the metal-semiconductor interface in the rows below. All images were taken on samples that featured the 40nm SiN_x capping layers and the BSG/ SiO_x APCVD doping stacks. However, for Ag (FT) many metal spots are detected at the Si wafer interface, while for Ag (NFT) such are much sparser. For AgAl (FT) much deeper contact features could be found, similar to locally alloyed BSF contacts of PERC solar cells, in accordance with literature.

3.5 Mechanical Adhesion of Electrodes

The results regarding adhesion of printed electrodes for surfaces with and without silicon nitride capping are shown in Fig. 5 where the given peel force values are the determined peak value per soldered pad, as fitted by a peak detection algorithm (*cf.* [8]). We used multiple samples for each combination.

For standard busbar interconnection peel forces are usually normalized to the ribbon width. However, as the wetted area during soldering seems to vary between pads, we choose not to normalize these values to the pad area (0.2 mm^2) or the wire/pad overlap area (0.06 mm^2). Instead we suggest to use the values of Ag (PERC) as a reference for sufficient adhesion strength.

For uncapped wafer surfaces, no strong correlation with the FFO set temperature is observed, except for the highest tested temperature $T_{\text{Set}} = 900 \text{ }^\circ\text{C}$, where most of the pastes seem to show a lower adhesion, hinting at slight overfiring. The results of the Ag (PERC) paste, already used in production, were comparable to the other materials. A notable exception is found in the Ag (FT) paste, which showed significantly higher values compared to the other pastes.

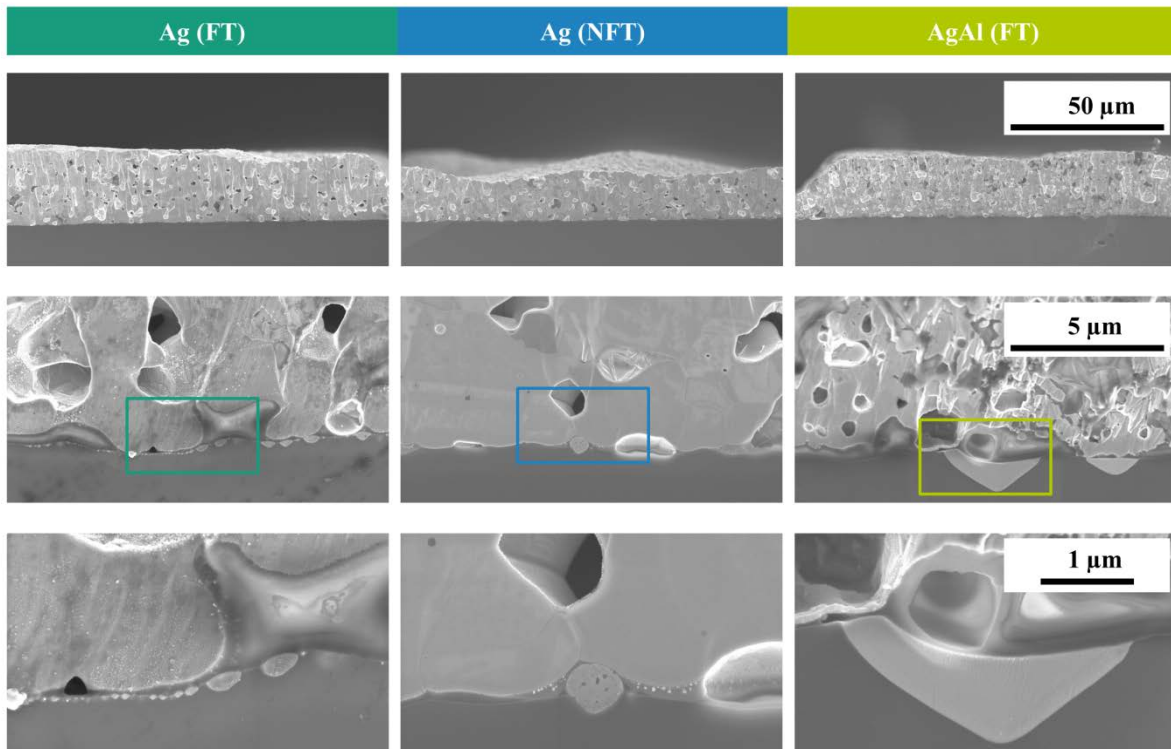


Figure 4: SEM images for exemplary investigation of contact formation for Ag (FT) (left column), Ag (NFT) (middle column) and AgAl (FT) (right column). Top row gives an overview of the metal finger, while middle and bottom row show exemplary magnification of the wafer-metal interface. All images taken on samples with 40 nm SiN_x and BSG/SiO_x stack.

For both, the AgAl (FT) and Ag (FT) paste, the detection ratio $n_{\text{Peaks}}/n_{\text{Pads}} > 95\%$ is very high at all conditions, indicating a reliable interconnection process.

For the samples capped with 100 nm SiN_x the peel forces are much smaller, in line with the higher detected contact resistivity. This again underlines that most pastes need a thinner SiN_x capping at the used thermal budget, at least on polished surfaces.

For further studies, Ag (FT) and AgAl (FT) will be tested on IBC solar cell precursors with the simpler fire through setup, which does not require separate contact opening processes.

4 CONCLUSION AND OUTLOOK

While many approaches rely on AgAl pastes for FT electrode formation on boron doping ($\rho_c = 5 \text{ m}\Omega \text{ cm}^2$ in this study with 100 nm SiN_x), we identify two Ag pastes forming contacts with a contact resistivity below $5 \text{ m}\Omega \text{ cm}^2$ on boron doping ($n_{\text{Surf}} = 3.1 \times 10^{19} \text{ cm}^{-3}$). Contact resistivity on phosphorus doping was very low on the highly doped ($n_{\text{Surf}} \geq 1.8 \times 10^{20} \text{ cm}^{-3}$) P profiles after co-diffusion ($\rho_c < 1 \text{ m}\Omega \text{ cm}^2$ for all Ag pastes).

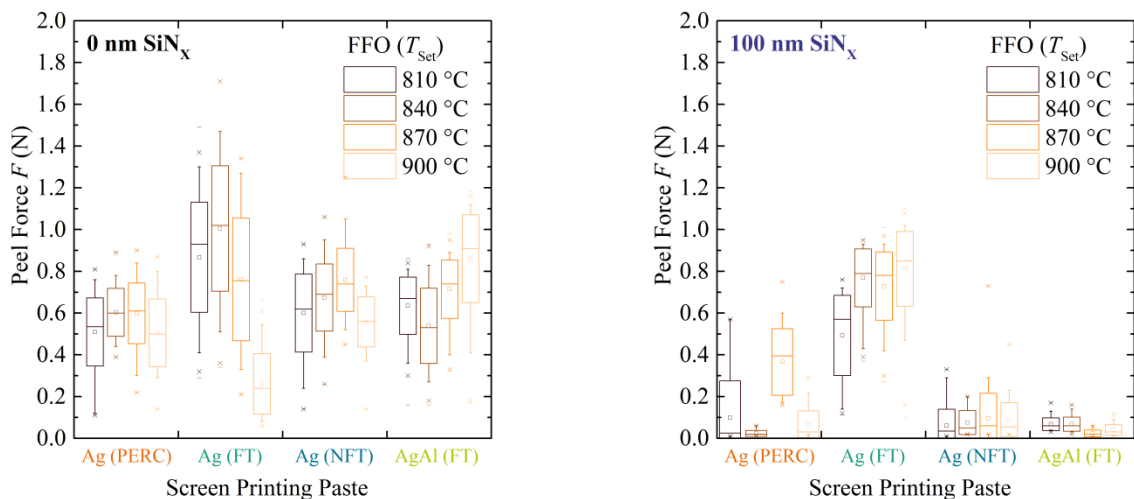


Figure 5: Measured peel force for all pastes at different FFO set temperatures. Left: Doped wafers without nitride capping, Right: Doped wafers with 100 nm SiN_x capping.

We also investigate the influence of dielectric layers on contact formation and varied the silicon nitride thickness, finding that one Ag paste is suitable as a FT paste, while another one is best used with defined local contact openings or thin SiN_x.

To further reduce manufacturing costs of IBC solar cells, we tested electrode designs, suitable for wire interconnection with Fraunhofer ISE's ultra-soft wave-shaped wires [9], resulting in less bowing, less breakage and straightforward module integration, and find high peel forces on small solder pads [10].

The integration of these promising processes into IBC solar cells will be investigated and published soon.

5 ACKNOWLEDGEMENTS

This work was supported by the German Federal Ministry for Economic Affairs and Energy within the research project "Backbone" under contract number 0324057B. The authors thank all coworkers at Fraunhofer ISE's PV-TEC and SCHMID facilities in Freudenstadt for assistance with sample processing, characterization and discussion; especially J. Schube for assistance with SEM measurements and J. Walter for peel force analyses.

J.D.H. acknowledges funding by the center of renewable energy of the University of Freiburg, within the interdisciplinary graduate school "DENE".

6 REFERENCES

- [1] VDMA, "International Technology Roadmap for Photovoltaic (ITRPV)," Ninth Edition 2018, 2018. [Online] Available: <http://www.itrpv.net/>.
- [2] T. Campbell, R. K. Kalia, A. Nakano, P. Vashishta, S. Ogata, and S. Rodgers, "Dynamics of Oxidation of Aluminum Nanoclusters using Variable Charge Molecular-Dynamics Simulations on Parallel Computers," *Physical Review Letters*, vol. 82, no. 24, pp. 4866–4869, 1999.
- [3] R. J. Schwartz and M. D. Lammert, "Silicon solar cells for high concentration applications," in *1975 International Electron Devices Meeting*, pp. 350–352.
- [4] D. Stüwe, D. Mager, D. Biro, and J. G. Korvink, "Inkjet technology for crystalline silicon photovoltaics," *Adv. Mater.*, vol. 27, no. 4, pp. 599–626, 2015.
- [5] J. D. Huyeng, A. Spribille, L. C. Rendler, C. Ebert, U. Eitner, and R. Keding, "Influence of interconnection concepts for IBC solar cell performance by simulation," in *SiliconPV 2018*, p. 20011.
- [6] D. K. Schroder and D. L. Meier, "Solar cell contact resistance—A review," *IEEE Trans. Electron Devices*, vol. 31, no. 5, pp. 637–647, 1984.
- [7] *Solarzellen - Datenblattangaben und Angaben zum Produkt für kristalline Silicium-Solarzellen*, EN 50461: 2007-03, 2007.
- [8] J. Walter, M. Tranitz, M. Volk, C. Ebert, and U. Eitner, "Multi-wire Interconnection of Busbar-free Solar Cells," *Energy Procedia*, vol. 55, pp. 380–388, 2014.
- [9] L. C. Rendler, J. Walter, A. Kraft, C. Ebert, S. Wiese, and U. Eitner, "Ultra-soft wires for direct soldering on finger grids of solar cells," *Energy Procedia*, vol. 124, pp. 478–483, 2017.
- [10] A. Spribille, J. D. Huyeng, T. Schweigstill, I. Franzetti, L. C. Rendler, and F. Clement, "Electrode design for wire interconnected back contact solar cells," in *this conference*.